Assessing mechanical properties of tissue phantoms with non-contact optical coherence elastography and Michelson interferometric vibrometry

Jiasong Li[1], Chih-Hao Liu[1], Alexander Schill[1], Manmohan Singh[1], Achuth Nair[1], Valery P. Zakharov[2], and Kirill V. Larin[1,2,3*]

[1] Department of Biomedical Engineering, University of Houston, TX, 77204, USA
[2] Department of Laser and Biotechnical Systems, Samara State Aerospace University, Samara, 443086, Russia
[3] Department of Molecular Physiology and Biophysics, Baylor College of Medicine, TX, 77030, USA

[*] **e-mail**: klarin@central.uh.edu

Abstract. *Purpose*: Elastography is an emerging method for detecting the pathological changes in tissue biomechanical properties caused by various diseases. In this study, we have compared two methods of noncontact optical elastography for quantifying Young's modulus of tissue-mimicking agar phantoms of various concentrations: a laser Michelson interferometric vibrometer and a phase-stabilized swept source optical coherence elastography system. *Methods*: The elasticity of the phantoms was estimated from the velocity of air-pulse induced elastic waves as measured by these two techniques. *Results*: The results show that both techniques were able to accurately assess the elasticity of the samples as compared to uniaxial mechanical compression testing. *Conclusion*: The laser Michelson interferometric vibrometer is significantly more cost-effective, but it cannot directly provide the elastic wave temporal profile, nor can it offer in-depth information. © 2016 Samara State Aerospace University (SSAU).

Keywords: optical coherence elastography, optical coherence tomography, laser Michelson interferometric vibrometer, elasticity, elastic wave, air-pulse, non-contact.

Paper #2809 received 2015.12.10; revised manuscript received 2015.12.25; accepted for publication 2015.12.30; published online 2016.02.01.

References

1. J. F. Greenleaf, M. Fatemi, and M. Insana, "Selected methods for imaging elastic properties of biological tissues," Annu Rev Biomed Eng 5, 57-78 (2003).
2. M. C. Chirambo, and D. Benezra, "Causes of blindness among students in blind school institutions in a developing country," Br J Ophthalmol 60(9), 665-8 (1976).
3. M. J. Paszek, N. Zahir, K. R. Johnson, J. N. Lakins, G. I. Rozenberg, A. Gefen, C. A. Reinhart-King, S. S. Margulies, M. Demb, D. Boettiger, D. A. Hammer, and V. M. Weaver, "Tensional homeostasis and the malignant phenotype," Cancer Cell 8(3), 241-54 (2005).
4. S. J. Zieman, V. Melenovsky, and D. A. Kass, "Mechanisms, pathophysiology, and therapy of arterial stiffness," Arterioscler Thromb Vasc Biol 25(5), 932-43 (2005).
5. J. S. Pepose, S. K. Feigenbaum, M. A. Qazi, J. P. Sanderson, and C. J. Roberts, "Changes in corneal biomechanics and intraocular pressure following LASIK using static, dynamic, and noncontact tonometry," Am J Ophthalmol 143(1), 39-47 (2007).
6. K. J. Parker, and R. M. Lerner, "Sonoelasticity of organs: shear waves ring a bell," J Ultrasound Med 11(8), 387-92 (1992).
7. R. Muthupillai, D. J. Lomas, P. J. Rossman, J. F. Greenleaf, A. Manduca, and R. L. Ehman, "Magnetic resonance elastography by direct visualization of propagating acoustic strain waves," Science 269(5232), 1854-7 (1995).

8. M. D'Onofrio, A. Gallotti, and R.P. Mucelli, "Tissue quantification with acoustic radiation force impulse imaging: Measurement repeatability and normal values in the healthy liver," AJR Am J Roentgenol 195(1), 132-6 (2010).
9. J. Bercoff, M. Tanter, and M. Fink, "Supersonic shear imaging: a new technique for soft tissue elasticity mapping," IEEE Trans Ultrason Ferroelectr Freq Control 51(4), 396-409 (2004).
10. G. Grabner, R. Eilmsteiner, C. Steindl, J. Ruckhofer, R. Mattioli, and W. Husinsky, "Dynamic corneal imaging," J Cataract Refract Surg 31(1), 163-74 (2005).
11. K. W. Hollman, S. Y. Emelianov, J. H. Neiss, G. Jotyan, G. J. Spooner, T. Juhasz, R. M. Kurtz, and M. O'Donnell, "Strain imaging of corneal tissue with an ultrasound elasticity microscope," Cornea 21(1), 68-73 (2002).
12. M. Tanter, D. Touboul, J. L. Gennisson, J. Bercoff, and M. Fink, "High-resolution quantitative imaging of cornea elasticity using supersonic shear imaging," IEEE Trans Med Imaging 28(12), 1881-93 (2009).
13. C. Li, Z. Huang, and R. K. Wang, "Elastic properties of soft tissue-mimicking phantoms assessed by combined use of laser ultrasonics and low coherence interferometry," Opt Express 19(11), 10153-63 (2011).
14. S. Wang, K. V. Larin, J. Li, S. Vantipalli, R. K. Manapuram, S. Aglyamov, S. Emelianov, and M. D. Twa, "A focused air-pulse system for optical-coherence-tomography-based measurements of tissue elasticity," Laser Phy Lett 10(7), 075605 (2013).
15. G. Scarcelli, and S. H. Yun, "In vivo Brillouin optical microscopy of the human eye," Opt Express 20(8), 9197-202 (2012).
16. G. Scarcelli, P. Kim, and S. H. Yun, "In vivo measurement of age-related stiffening in the crystalline lens by Brillouin optical microscopy," Biophys J 101(6), 1539-45 (2011).
17. J. Schmitt, "OCT elastography: imaging microscopic deformation and strain of tissue," Opt Express 3(6), 199-211 (1998).
18. S. Wang, and K. V. Larin, "Optical coherence elastography for tissue characterization: a review," J Biophotonics 8(4), 279-302 (2015).
19. D. Huang, E. A. Swanson, C. P. Lin, J. S. Schuman, W. G. Stinson, W. Chang, M. R. Hee, T. Flotte, K. Gregory, C. A. Puliafito, and J. G. Fojimoto, "Optical coherence tomography," Science 254(5035), 1178-81 (1991).
20. M. Sticker, C. K. Hitzenberger, R. Leitgeb, and A. F. Fercher, "Quantitative differential phase measurement and imaging in transparent and turbid media by optical coherence tomography," Opt Lett 26(8), 518-20 (2001).
21. S. Wang, J. Li, R. K. Manapuram, F. M. Menodiado, D. R. Ingram, M. D. Twa, A. J. Lazar, D. C. Lev, R. E. Pollock, and K. V. Larin, "Noncontact measurement of elasticity for the detection of soft-tissue tumors using phase-sensitive optical coherence tomography combined with a focused air-puff system," Opt Lett 37(24), 5184-6 (2012).
22. X. Zhang, and J. F. Greenleaf, "Estimation of tissue's elasticity with surface wave speed," J Acoust Soc Am 122(5), 2522-5 (2007).
23. Z. Han, J. Li, M. Singh, C. Wu, C. H. Liu, S. Wang, R. Idugboe, R. Raghunathan, N. Sudheendran, S. R. Aglyamov, M. D. Twa, and K. V. Larin, "Quantitative methods for reconstructing tissue biomechanical properties in optical coherence elastography: a comparison study," Phys Med Biol 60(9), 3531-47 (2015).
24. L. Drain, The laser Doppler technique, John Wiley, Chichester, 186-194 (1980). ISBN: ISBN 0-471-27627-8.
25. P. Castellini, G. Revel, and E. Tomasini, "Laser Doppler vibrometry: a review of advances and applications," The Shock and vibration digest 30(6), 443-456 (1998).
26. G. R. Ball, A. Huber, and R. Goode, "Scanning laser Doppler vibrometry of the middle ear ossicles," Ear Nose Throat J 76(4), 213-222 (1997).
27. J. Sokołowski, K. Niemczyk, R. Bartoszewicz, K. Morawski, A. Bruzgielewicz, and B. Rygalska, "Round window's movability measurements with helping of LDV in evaluation of ossicular chain functioning," Otolaryngol Pol 64(7), 77-80 (2010).
28. B. Felver, D. C. King, S. C. Lea, G. J. Price, and A. D. Walmsley, "Cavitation occurrence around ultrasonic dental scalers," Ultrason Sonochem 16(5), 692-7 (2009).
29. S. C. Lea, A. D. Walmsley, P. J. Lumley, and G. Landini, "A new insight into the oscillation characteristics of endosonic files used in dentistry," Phys Med Biol 49(10), 2095-102 (2004).
30. M. De Melis, U. Morbiducci, and L. Scalise, "Identification of cardiac events by optical Vibrocardiograpy: comparison with Phonocardiography," Conf Proc IEEE Eng Med Biol Soc 2007, 2956-9 (2007).
31. U. Morbiducci, L. Scalise, M. De Melis, and M. Grigioni, "Optical vibrocardiography: a novel tool for the optical monitoring of cardiac activity," Ann Biomed Eng 35(1), 45-58 (2007).
32. L. Scalise, and U. Morbiducci, "Non-contact cardiac monitoring from carotid artery using optical vibrocardiography," Med Eng Phys 30(4), 490-7 (2008).
33. D. Rixen, and T. Schuurman, "In Vivo Measurement of the Human Thorax and Abdomen Surface Using Laser Vibrometry: A New Diagnostic Tool?" in Topics in Modal Analysis II, Volume 6, Springer, New York, 235-245 (2012).

34. Y. Yazicioglu, T. J. Royston, T. Spohnholtz, B. Martin, F. Loth, and H. S. Bassiouny, "Acoustic radiation from a fluid-filled, subsurface vascular tube with internal turbulent flow due to a constriction," J Acoust Soc Am 118(2), 1193-209 (2005).
35. M. De Melis, U. Morbiducci, L. Scalise, E. P. Tomasini, D. Delbeke, R. Baets, L. M. Van Bortel, and P. Segers, "A noncontact approach for the evaluation of large artery stiffness: a preliminary study," Am J Hypertens 21(12), 1280-3 (2008).
36. M. C. Dahl, P. A. Kramer, P. G. Reinhall, S. K. Benirschke, S. T. Hansen, and R. P. Ching, "The efficacy of using vibrometry to detect osteointegration of the Agility total ankle," J Biomech 43(9), 1840-3 (2010).
37. P. Castellini, R. Huebner, and M. Pinotti, "Vibration measurement on artificial heart valve by laser doppler vibrometry," Fifth International Conference on Vibration Measurements by Laser Techniques, International Society for Optics and Photonics (2002).
38. C. C. Rondini, G. L. Rossi, and L. Scalise, "Laser vibrometry and stress measurement by thermoelasticity on mechanical heart valve," Sixth International Conference on Vibration Measurements by Laser Techniques: Advances and Applications, International Society for Optics and Photonics (2004).
39. R. K. Manapuram, V. G. R. Manne, and K. V. Larin, "Development of phase-stabilized swept-source OCT for the ultrasensitive quantification of microbubbles," Laser Physics 18(9), 1080-1086 (2008).
40. J. Li, S. Wang, R. K. Manapuram, M. Singh, F. M. Menodiado, S. Aglyamov, S. Emelianov, M. D. Twa, and K. V. Larin, "Dynamic optical coherence tomography measurements of elastic wave propagation in tissue-mimicking phantoms and mouse cornea in vivo," J Biomed Opt 18(12), 121503 (2013).
41. S. Wang, and K. V. Larin, "Shear wave imaging optical coherence tomography (SWI-OCT) for ocular tissue biomechanics," Opt Lett 39(1), 41-4 (2014).
42. S. Wang S, A. L. Lopez 3rd, Y. Morikawa, G. Tao, J. Li, I. V. Larina, J. F. Martin, and K. V. Larin, "Noncontact quantitative biomechanical characterization of cardiac muscle using shear wave imaging optical coherence tomography," Biomed Opt Express 5(7), 1980-92 (2014).
43. A. R. Skovoroda, S. Y. Emelianov, and M. O'Donnell, "Tissue elasticity reconstruction based on ultrasonic displacement and strain images," IEEE Trans Ultrason, Ferroelect, Freq Control 42(4), 747-765 (1995).
44. J. F. Doyle, Wave Propagation in Structures: Spectral Analysis Using Fast Discrete Fourier Transforms, 2nd ed., Springer-Verlag, New York (1997). ISBN: 0387949402.
45. K. M. Kennedy, L. Chin, R. A. McLaughlin, B. Latham, C. M. Saunders, D. D. Sampson, and B. F. Kennedy, "Quantitative micro-elastography: imaging of tissue elasticity using compression optical coherence elastography," Sci Rep 5, 15538 (2015).
46. S. Wang, and K. V. Larin, "Noncontact depth-resolved micro-scale optical coherence elastography of the cornea," Biomed Opt Express 5(11), 3807-21 (2014).
47. M. Singh, C. Wu, C. H. Liu, J. Li, A. Schill, A. Nair, and K. V. Larin, "Phase-sensitive optical coherence elastography at 1.5 million A-Lines per second," Opt Lett 40(11), 2588-91 (2015).
48. R. W. Kirk, B. F. Kennedy, D. D. Sampson, and R. A. McLaughlin, "Near Video-Rate Optical Coherence Elastography by Acceleration With a Graphics Processing Unit," J Lightwave Technol 33(16), 3481-3485 (2015).

1 Introduction

The biomechanical properties of tissues are important parameters for tissue characterization [1]. For example, keratoconus structurally degenerates the cornea [2], tumors generally stiffen tissue [3], and atherosclerosis hardens the vasculature [4]. Thus, quantifying changes of biomechanical properties of tissue can provide critical information for early diagnosis and effective treatment of various diseases [3, 5].

Several elastographic methods have been developed in the past few decades to characterize the biomechanical properties of tissues, such as ultrasound elastography (USE) [6], magnetic resonance elastography (MRE) [7], acoustic radiation force imaging [8], supersonic shear imaging [9], and dynamic corneal imaging [10]. All of these methods combine an imaging technique with external loading, such as mechanical compression [11], acoustic radiation force [12], pulsed laser [13], or focused air-pulse [14]. The imaging modalities measure the tissue response to the excitation, and these measurements can then characterize the biomechanical properties of tissue through the use of appropriate mechanical models. However, these elastographic methods require relatively large tissue deformation due to their limited displacement sensitivity. Alternatively, Brillouin microscopy can map the Brillouin shift of tissue in 3D with high spatial resolution without external loading [15, 16]. While it is understood that the Brillouin shift is related to the Young's modulus, accurately quantifying the stiffness of tissue from the Brillouin shift is still a challenge.

Optical coherence elastography (OCE) is an emerging technique that can assess the biomechanical properties of tissues completely non-destructively [17, 18]. Similar to USE and MRE, OCE is an elastographic extension of its parent imaging modality, optical coherence tomography (OCT) [19]. In addition to

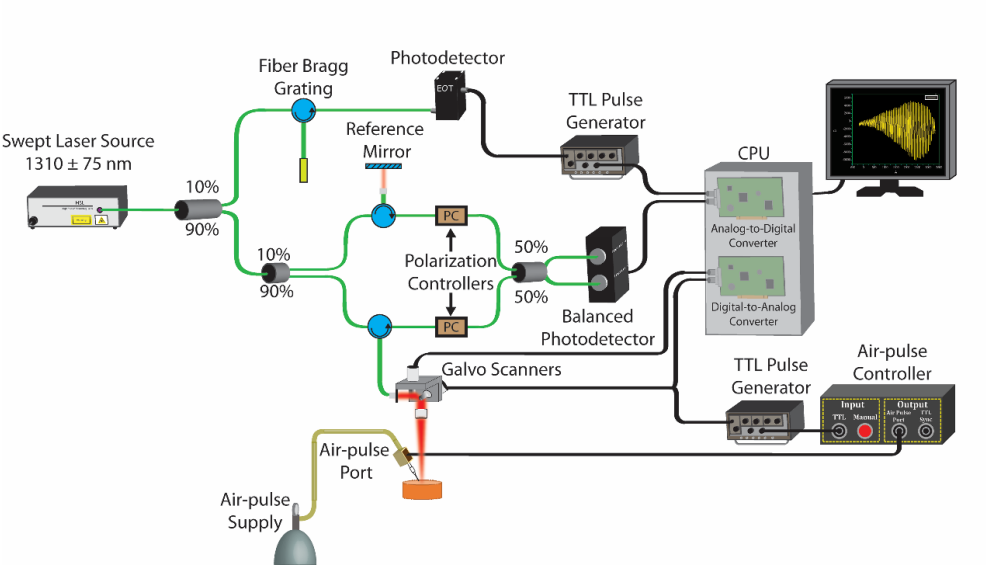

Fig. 1 Schematic of PhS-SSOCE experimental setup.

micrometer-scale spatial resolution, phase-resolved OCT has enabled nanometer-scale displacement sensitivity [20]. We have previously utilized the superior displacement sensitivity of OCT to analyze the propagation of a low amplitude (≤ 10 μm) focused air-pulse induced elastic wave [21]. By quantifying the velocity, the Young's modulus can then be estimated with reasonable accuracy as compared to uniaxial mechanical testing [22, 23].

However, OCT setups, particularly phase-sensitive systems, can be complex and expensive. Simpler and more cost-effective techniques such as Michelson interferometer-based laser vibrometery could potentially also provide measurements for calculating the velocity of the air-pulse induced elastic wave [24]. Laser vibrometry has been successfully used in various applications due to its high sensitivity, which has enabled detection of very small vibrations on the order of the source wavelength. Laser vibrometry was first applied in different engineering fields, such as modal analysis, vibration and noise testing, characterizing loudspeakers, and assessing piezoceramic transducers [25]. Recently, laser vibrometry has gained traction in biomedical and bioengineering applications, such as auditory research [26, 27], dentistry [28, 29], cardiology [30-32], as well as elastography and rheology [33-38].

In this study, a phase sensitive swept source optical coherence elastography (PhS-SSOCE) system and laser Michelson interferometric vibrometer (LMIV), both developed in our lab, were utilized to measure the velocity of focused air-pulse induced elastic waves propagating in tissue-mimicking agar phantoms of various concentrations. The Young's modulus was then quantified from the wave velocity and was compared to the stiffness as measured by uniaxial mechanical compression testing. The results show that the velocities as measured by both systems were very similar, and the estimated Young's modulus was consistent with mechanical testing.

2 Materials and methods

A home-built focused air-pulse delivery system [14] induced elastic waves in tissue-mimicking agar phantoms of various concentrations (1%, 1.5%, 2%, w/w, n=3 for each concentration) The elastic waves were then detected by the LMIV and PhS-SSOCE systems, separately. The air-pulse delivery system employed an air gate and a control unit to provide a short duration (~800 μs) focused air-pulse to the sample surface, and the control unit enabled synchronization of the air-pulse with the OCE and LMIV systems. The air source pressure was obtained from a standard pressure gauge, and the air-pulse was expelled through a cannula port with a flat edge and inner diameter of ~150 μm. The localized air-pulse excitation was precisely positioned with a 3D linear micrometer stage.

The PhS-SSOCE system was comprised of the previously described air-pulse delivery device and a home-built phase stabilized swept source optical coherence tomography (PhS-SSOCT) system. A schematic of the experimental setup is displayed in Fig. 1. Further details about the PhS-SSOCT system can be found in our previous work [39, 40]. Briefly, the PhS-SSOCT system utilized a broadband swept laser source (HSL2000, Santec, Inc., Torrance, California) with central wavelength of 1310 nm, bandwidth of ~130 μm, scan rate of 30 kHz, and output power of ~39 mW. A fiber Bragg grating was used as the A-scan trigger that improved phase stabilization. The axial and lateral resolutions of the system were ~11 μm and ~16 μm, respectively. The phase stability of the system was ~16 milliradians, which corresponded to ~3.3 nm displacement sensitivity in air. The experimental acquisition and data processing methods are detailed in our previous work [41]. Simply, successive M-mode images were acquired in a line, and the M-mode frame trigger was synchronized with the air-pulse so that effectively, the same elastic wave was imaged.

LMIV schematic is depicted in Fig. 2. The LMIV employed a Helium-Neon (HeNe) laser with wavelength of 633 nm and output power of 1.5 mW (model 31005, Research Electro-Optics, Inc., Boulder, CO). The output of the HeNe laser was expanded and collimated to 90% of the objective lens aperture to maximize photon collection. The light beam was then split into sample and reference arms using a 50:50 non-polarizing cube beam splitter. In the sample arm, the beam was transmitted through a 10X microscope objective and focused on the sample surface. In the reference arm, the beam was directed to a matching 10X microscope objective and focused onto the surface of a silver mirror. After the reflected light beam passed through the beam splitter, the interference signal was detected by a silicon photodetector (model DET100A, Thorlabs, Inc., USA). The temporal intensity output from the photodetector was captured by a digital oscilloscope (model DS4014, Rigol Inc., USA). The air-pulse stimulation and the data acquisition were synchronized by a TTL signal, which was provided by a digital pulse generator (model 575, BNC Inc., USA). The system was assembled on a 3-inch thick optical breadboard and supported with four sorbothane isolation pads to maximize system stability and minimize environmental noise. During the LMIV measurements, all data was acquired with the same acquisition window and oscilloscope sampling settings. Six co-linear measurements positions were recorded on each sample, and the distance between two adjacent positions was 1 mm. The time t for the wave to propagate from a reference measurement position to each location was obtained by cross-correlation analysis. The elastic wave velocity, c, was then obtained by the inverse slope of the linear fit of the propagation distances, Δd, to the elastic wave propagation delays, Δt [42].

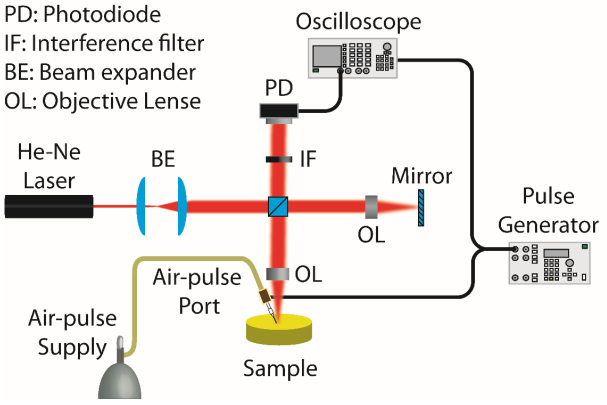

Fig. 2 Schematic of LMIV experimental setup.

Since the tissue-mimicking agar phantoms can be treated as an isotropic homogeneous elastic material, the Young's modulus [43], E, was estimated by [23, 40, 44]:

$$E = 2\rho c^2 \frac{(1+v)^3}{(0.87+1.12v)^2}, \quad (1)$$

where ρ=1.02 k/gm^3 was the material density, and v=0.49 [21, 44] was the Poisson ratio. For all experiments, the output pressure of the air-pulse was ≤ 10 Pa. Uniaxial mechanical compression testing (model 5943, Instron Inc., MA, USA) was performed on the same samples after OCE and LMIV measurement [23].

3 Results

Figure 3 shows typical 1% agar phantom surface response signal to the air-pulse at various positions during OCE (Fig. 3(a)) and LMIV (Fig. 3(b)) measurement. During OCE measurements, 501 M-mode measurements were acquired over 6.9 mm. Figure 3(a) shows typical surface responses to the air-pulse stimulation at OCE measurement positions which were 0.1 mm apart, and the first acquisition position was 1 mm away from the excitation position. During LMIV experiments, the first measurement position was also 1 mm away from the stimulation position, but successive measurement positions were 1 mm apart as depicted in Fig. 3(b).

Figure 4 shows the elastic wave propagation velocity as measured by both systems. The group velocity as measured by OCE was 1.72±0.25 m/s, 3.41±0.49 m/s, and 5.11±0.26 m/s in the 1%, 1.5%, and 2% agar phantoms, respectively. The velocities measured by the LMIV from the same agar samples were 1.75±0.03 m/s, 3.66±0.26 m/s, and 5.13±0.28 m/s, respectively. Statistical testing by a paired t-test showed no significant difference between the two systems (P=0.90, 0.25, and 0.89 for the 1%, 1.5%, and 2% phantoms, respectively).

Figure 5 shows the Young's modulus (E) of the samples estimated based on the OCE and LMIV measurements using equation (1) and as measured by "gold standard" mechanical testing system. The Young's moduli of the 1%, 1.5%, and 2% agar phantoms as estimated by OCE were 8.01±2.3 kPa, 31.39±9.19 kPa, and 69.45±7.07 kPa, respectively. The elasticities as quantified by the LMIV were 8.12±0.28 kPa, 35.69±5.07 kPa, and 70.14±7.57 kPa for the 1%, 1.5%, and 2% phantoms, respectively. The stiffness of the same samples was also measured by mechanical testing (MT), which resulted in a stiffness of 9.46±0.43 kPa, 45.34±2.32 kPa, and 89.25±9.4 kPa for the 1%, 1.5%, and 2% samples, respectively.

4 Discussion

The shape of the displacement as measured by the LMIV (Fig. 3(b)) was somewhat similar to the displacements detected by the OCE system in this work (Fig. 3(a)) and previous work [23, 40]. The differences in the shape of the temporal profiles can be attributed to the different ways of each technique measure the

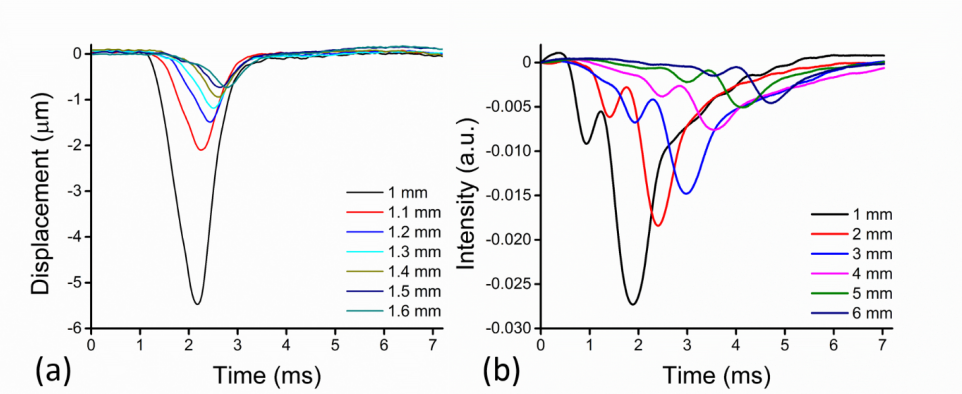

Fig. 3 Sample surface responses of a 1% agar phantom recorded during (a) OCE and (b) LMIV experiment at the indicated distances from the air-pulse excitation.

displacement of the sample. OCE measures the optical path difference between sample and reference arm, and the LMIV measures the intensity of light reflected from the sample surface. More specifically, the elastic wave may undulate similar to a wave in water, and the resulting change in sample surface geometry relative to incident beam may explain the kink during the inward process. Furthermore, OCE can easily provide absolute displacement, which can be used in other OCE techniques, such as compressional OCE for stress/strain analysis [45].

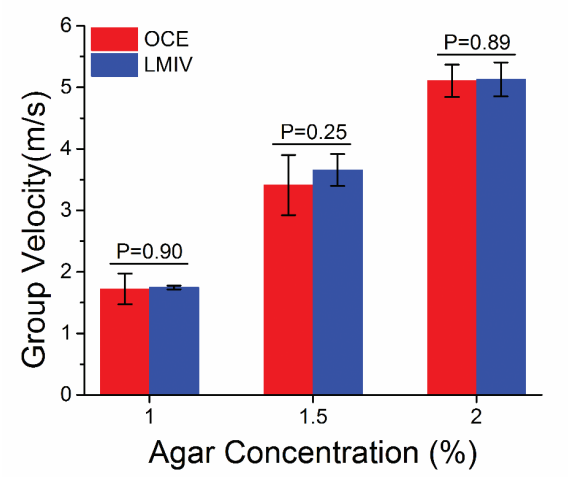

Fig. 4 Elastic wave propagation velocity measured by OCE and LMIV. Statistical testing was performed by a paired t-test to demonstrate that the velocity measurements made by both systems were not different. The respective *P*-values are labeled.

Statistical testing via a paired t-test showed that there was no significant difference between the velocities measured by both systems, with P=0.90, 0.25, and 0.89 for the 1%, 1.5%, and 2% phantoms, respectively (Fig. 4). However, the LMIV can only measure the wave propagation at the surface of the sample since internal scattering is dominated by the specular reflection from the surface. In contrast, OCE can provide depth-resolved elasticity measurements [46]. To further demonstrate the depth-resolved elasticity characterization by OCE, a sandwich-type agar phantom was constructed with a 2% agar layer between two layers of 1% agar (Fig. 6). Because the air-pulse induced elastic wave wavelength is large, spectral analysis was utilized to provide depth-resolved elasticity assessment [46], and all three layers were differentiated successfully. Figure 6 shows the phase velocity of the air-pulse induced elastic wave at 180 Hz. The boundary layers are marked by the dashed red line.

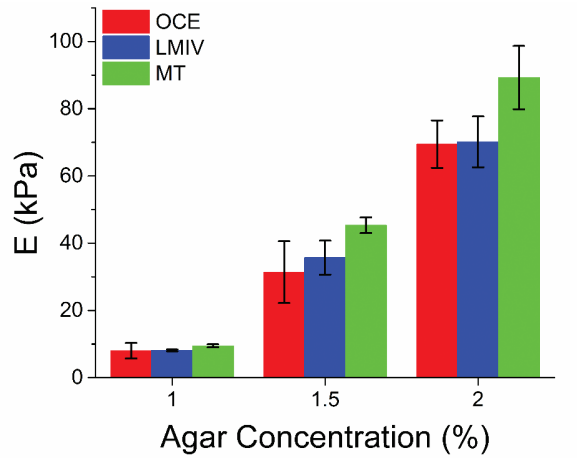

Fig. 5 Young's modulus (E) estimated by the OCE system, LMIV, and as measured by mechanical testing (MT).

The Young's moduli estimated from the group velocities were smaller than as measured by mechanical testing. However, this is in agreement with our very recent investigation and can be explained by assumptions about sample geometry in Eq. 2 and the non-linearity of the agar stress-strain curve [23].

The LMIV can provide very rapid detection of elasticity since the data acquisition and post-processing are minimal. During OCE study, 501 successive M-mode images were acquired at 100 ms per M-mode image, resulting in an acquisition time of approximately half a minute. However, due to the large data size, the post-processing time can be on the order of several minutes. Since each OCE measurement position results in a longer acquisition time and more data, there is an

intrinsic trade-off between spatial resolution and acquisition and processing times. Lateral measurements in the LMIV system were made by translating the sample, whereas the galvanometer-mounted mirrors were used to make measurements at the transverse locations in the OCE system. An automated motorized linear stage would dramatically speed up the acquisition time of the LMIV, but the speed would be limited to ensure that no damage was caused to the sample or that there was no slipping of the sample. Hence, elastographic measurements made with OCE are simpler because the probe beam is moved and not the sample. Furthermore, the LMIV requires precise alignment in order to capture the reflected photons. Moreover, OCE can provide a depth-resolved image of the sample, making alignment significantly easier.

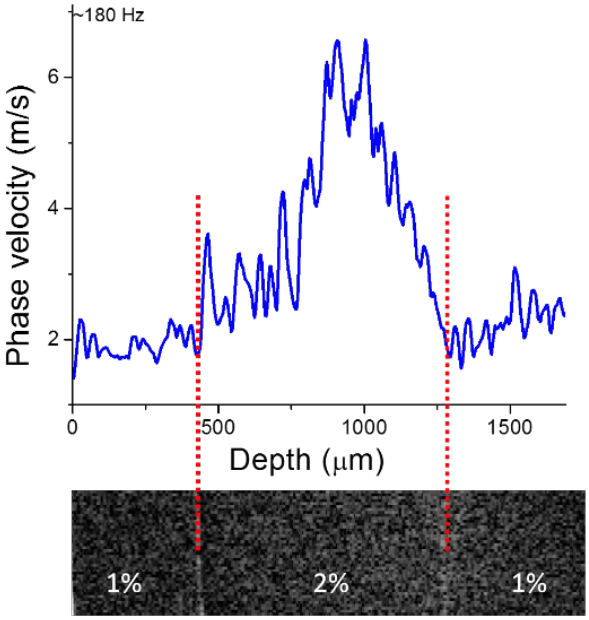

Fig. 6 Phase velocity of the air-pulse induced elastic wave at 180 Hz in a sandwich-type agar phantom (top) with OCT image of the phantom (bottom). The layer boundaries are marked by the dashed red line.

In this study, successive M-mode images were acquired and an air-pulse excitation was synchronized with each measurement. This technique may not be feasible for *in vivo* measurement due to multiple excitations and the extended acquisition time, which may lead to excessive laser exposure. However, we have recently developed a technique that takes advantage of recent advances in OCT sources by directly imaging the propagation of an air-pulse induced elastic wave. Here, only a single excitation was necessary for a line measurement and the MPE limit for the sample (cornea) was not exceeded [47]. However, the spatial and temporal resolutions were still limited as compared to the OCE technique described in this work. Recently, GPU-accelerated compressional OCE has been demonstrated, enabling near real-time 3D elasticity assessment [48]. Combining high-performance computing would drastically reduce the processing time of the OCE post-processing and would also enable near real-time characterization of tissue biomechanical properties and is currently under development.

Another core issue for comparison of the two techniques is the cost. The approximate total costs of building the OCE and LMIV systems are listed in Table 1. The LMIV system is approximately one-tenth the cost of the OCE system. The LMIV system requires a simple HeNe laser, whereas the OCE system requires a broadband low coherence swept source laser. As the LMIV system is an open space system, there are no expensive fiber based components. Fiber optical components are becoming more mainstream and prices continue to decrease. However, the price disparity will still exist due to the sheer difference in complexity of the two systems.

Table 1. Approximate cost in $US of the OCE and LMIV systems used in this study

	OCE	**LMIV**
Light source	20000	850
Optical components	4500	2550
Scan	2850	0
Control units	6500	600
Data acquisition	10000	150
Data processing	3000	500
Total cost	46850	4650

5 Conclusion

In this work we have utilized two optical techniques, laser Michelson interferometric vibrometry (LMIV) and optical coherence elastography (OCE) to assess the elasticity of tissue-mimicking agar phantoms. A focused air-pulse induced elastic waves in the samples, which were then detected by the two techniques. The stiffness of the agar phantoms as quantified from the velocity were measured by the LMIV and OCE systems was in good agreement. The LMIV system was significantly less complex and cost-effective as compared to the OCE system, but the LMIV system cannot provide-depth resolved elasticity assessment. Therefore, if depth-resolved elasticity or high spatial resolutions are not necessary, then LMIV may be a simple and cost-effective technique to measure the elasticity of tissues completely noninvasively.